Inductive Loop Operation versus Loop Antenna for Partial Discharge Detection

Sana Chouaibi[1,3], Mohamed Hadj Said[3], Antonino Imburgia[2], Pietro Romano[2], Sinda Kaziz[2,3], Guido Ala[2], Mossaad Ben Ayed[1], Denis Flandre[4], Fares Tounsi[4*]

[1]*National Engineering School of Sousse (ENISo), Sousse University, Tunisia*
[2]*L.E.PR.E. H.V. Laboratory, Department of Engineering, University of Palermo, Italy*
[3]*Center for Research in Microelectronics & Nanotechnology (CRMN), Sousse, Tunisia*
[4]*SMALL Group, ICTEAM Institute, Université catholique de Louvain, Belgium*

*Corresponding author: *fares.tounsi@uclouvain.be*

Abstract—This article delves into the application and efficacy of planar loop sensors for detecting partial discharge (PD) phenomena. The preference for loop sensors in PD detection stems from their simple design, non-destructive testing feature, and contactless characteristics. The paper explores both experimental and finite element modeling (FEM) approaches to evaluate the performance of distinct planar square spiral sensors in PD detection. The primary objective of the study is to compare inductive loops with loop antennas by varying the geometric parameters to achieve each approach. Two single-turn square loop antennas were designed, with a circumference of 30 cm and 75 cm, and compared with four multi-turn square inductive loops with an exterior side of 31.2 mm and varying geometric parameters. The figures of merit of all sensors, such as inductance, quality factor, and resonant frequency, are extracted through measurement and simulation to identify the most influential parameter that maximizes the sensing capability toward PD.

Keywords—Partial discharge detection, Loop antenna, Inductive loop, Quality factor, Planar inductance.

I. INTRODUCTION

In the realm of electrical engineering, loop sensors have emerged as versatile components with applications spanning various fields. These sensors, characterized by their closed-loop structure, find use in different areas, such as traffic management, communication systems, magnetic resonance imaging (MRI), and radio frequency identification (RFID) systems. Their standard advantages, featuring a simple structure, immunity to human body movements, and simple manufacturing process, make them a predominant choice in various applications, such as wireless charging systems or proximity sensing with a non-destructive testing (NDT) approach. For instance, loop sensors have proven effective in detecting partial discharge (PD) defects in electrical networks [1], indicative of insulation degradation and potential equipment failure, which pose significant threats to the reliability and safety of expensive electrical equipment such as power transformers, gas-insulated switchgear (GIS), and medium voltage alternating current (MVAC) cable.

Several research papers have delved into the identification of PD through the use of loop sensors, leading to proof of their detection capability [2-5]. Since these coils can be designed in various shapes, such as rectangular, circular, and meander, they have advantages and limitations. Suo *et al.* investigated PD detection in GIS using a square magnetic loop structure [6]. The probe, which is 166 mm long, 104 mm wide, and 2 mm thick, is designed to operate in the 10–200 MHz range since the PD electromagnetic emission spectrum falls into this band. The results show that at a distance of 20 cm from the discharge source, the probe induces a voltage of 0.65 V, and the PD spectrum is mainly concentrated below 200 MHz. The paper confirms that the magnetic loop probe has good frequency response characteristics and high immunity to interference in near-field detection. Kaziz *et al.* conducted an extensive study on inductive loop sensors for PD detection along high-voltage transmission cables [2]. They examined three sensor topologies, including spiral, non-spiral, and meander shapes, all sketched on FR-4 printed circuit boards (PCBs). This research aimed to find the optimal geometry of inductive sensors to improve their sensitivity and selectivity for effective PD detection. Imburgia *et al.* focused on evaluating different inductive loop topologies, which were also printed on an FR-4 substrate [7]. These sensors were tested to evaluate their ability to detect three types of PD: corona, surface, and internal discharge. The experiment results showed that the spiral inductive shape has the highest sensitivity for detecting PD, while the meander shape has the lowest. The frequency spectrum of the three sensors' outputs falls between 10 MHz and 45 MHz. Overall, the results show that loop sensors are suitable for PD detection in high-voltage equipment and power modules. All these studies highlighted the importance of designing simple loop sensors tailored to detect different types of PD, which could be crucial in various industrial applications [5]. In fact, PCB-based loop sensors offer lightweight, compact, better signal-to-noise ratio, and low-cost solutions for PD detection compared to other commercial sensors. Another breakthrough was achieved using an integrated loop antenna based on a square planar inductor and resonant at about 5 MHz [8]. This latter demonstrated its ability to detect corona discharges by delivering a damped-sinusoidal induced voltage of approximately 100 mV amplitude at a distance of 5 cm when using a 60 dB gain amplifier.

The geometric configuration of a loop sensor, which includes parameters such as the number of turns, diameter, spiral width, separation between tracks, and orientation, has a significant impact on its sensitivity. Moreover, properly understanding whether the sensor relies on the operation of an inductive loop or a loop antenna is essential to optimizing these geometric factors. To take full advantage of these loop sensors, we're delving into theoretical frameworks and experimental methods for engineering optimization in order to enhance sensor sensitivity towards PD pulses. The paper is organized as follows: Section II discusses the design of loop antennas, while Section III deals with the design of the inductive loops. Section IV describes the PD detection setup, with parameter extraction detailed in Section V. Section VI concludes with results and a discussion about PD detection.

2024 IEEE 5th International Conference on Dielectrics (ICD) | 979-8-3503-0897-6/24/$31.00 ©2024 IEEE | DOI: 10.1109/ICD59037.2024.10613039

II. LOOP ANTENNAS DESIGN

As a first step, a loop antenna, generally used in communication systems (broadcasting and receiving), will be designed and used to measure the magnetic component of the emitted electromagnetic field by the PD source. Loop antennas can be classified into two types: electrically-large loop antennas (also known as resonant antennas) and electrically-small loop antennas (known as magnetic antennas or loops) [9]. In the former, the circumference of the resonant antenna loop is approximately equal to the free space wavelength (λ) of the signal to be measured, while in the latter, the circumference is much less than the signal wavelength (ideally a tenth), ensuring that the current flowing through all wires remains uniform and in phase.

On the other hand, researchers have proven that when the discharge source is not included in the metal casings, which can cause multiple reflections, PDs (corona, surface, and internal discharges) in medium- and high-voltage apparatus have an EM emission frequency of 1 to 100 MHz (corresponding to λ from 3 m to 300 m). Hence, towards the short-wave range, the size of the antenna becomes more bulky and therefore constitutes a major constraint that pushes us to opt for electrically small loops. In contrast to a large antenna, small loop antennas have: (i) a low radiation resistance (milli- or micro-Ω range) compared to their loss resistance (hundreds ratio), which leads to low radiation efficiency due to high power losses in the conductors forming the loop in the form of heat; and (ii) a high inductive reactance, so that their impedance is difficult to match to the transmitter, which means they perform better as receiving antennas (particularly for loops with a circumference smaller than about a tenth wavelength) at lower frequencies. Nonetheless, small loops are very effective as receivers in noisy environments for low-frequency magnetic fields because they maintain a very good signal-to-noise ratio [10].

In that respect, two single-turn square loop antennas were designed, with a circumference of 30 cm (corresponding to f = 100 MHz) and 75 cm (corresponding to f = 40 MHz). These two sensors will function as an electrically small loop antenna, operating in the near-field region within the high frequency (HF) and very high frequency (VHF) bands. The two antennas, shown in Fig. 1, were patterned on an FR4-based PCB with a relative dielectric constant of 4.4 and a copper thickness of 17 µm, using an 'LPKF ProtoMat S63' prototyping machine. The geometric dimensions of these loop antennas are outlined in Table I, encompassing parameters such as the outer side (D) and the track width (w). The lumped equivalent electrical model of the loop antenna (shown in Fig. 2) consists of a resistance (R_s) in series with a self-inductance (L_s), both of which are parallel to a capacitance (C_s). In addition to the typical electrical resistance, R_{loss}, series resistance in the electrically small loop antennas includes low radiation resistance, R_{rad}, dwarfed by ohmic losses (resulting in low antenna efficiency), as given by [10]:

$$R_{rad} = \eta \left(\frac{2\pi}{3}\right)\left(n\frac{kA}{\lambda}\right)^2 = 320\,\pi^4 \left(n\frac{A}{\lambda^2}\right)^2 \qquad (1)$$

where η=120π is the wave impedance of the free space (or Z_o), k is the wavenumber (2π/λ), and A is the area enclosed by the loop. For a given wavelength, the radiation resistance of loop antennas, and consequently the radiated power, increases proportionally to the square of the area and can be improved by adding more turns to the detriment of losses. For the proposed square antennas, radiation resistance, which mainly depends on the electrical size of the loop, is evaluated at mΩ for both designs.

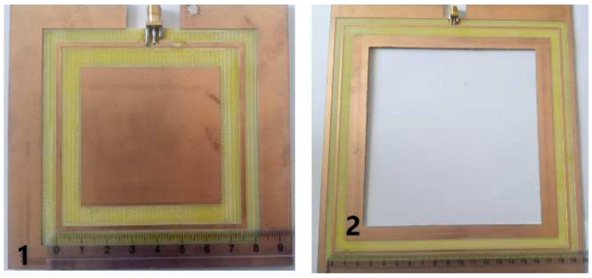

Fig. 1. Manufactured single-turn loop antenna with a circumference of: (a) 30 cm, and (b) 75 cm.

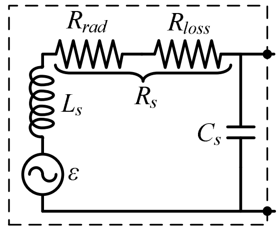

Fig. 2 The lumped equivalent electrical model of the manufactured electrically-small loop antenna (for frequencies below resonance).

TABLE I. GEOMETRICAL DIMENSIONS OF THE LOOP ANTENNAS.

Loop	D (mm)	w (mm)	Circumference (m)	λ/10 (MHz)
1	75	2	0.30	100
2	187.5	2	0.75	40

III. INDUCTIVE LOOPS DESIGN

To serve the same purpose, four square planar inductive loops, shown in Fig. 3, were designed with the aim of assessing their aptitude for detecting PD and exploring the effect of their dimensions and shapes on their sensitivity. Table II presents the inductive loop geometric dimensions, where n is the number of turns, D and d are the outer and inner sides, respectively, and w and s are the track width and spacing, respectively. An induction or inductive loop is an electromagnetic communication or detection system that is based on Faraday's law of induction. The inductive loop is one of the simplest, most versatile, and best-known types of magnetic field sensors. Their transfer function $\varepsilon = f(B)$ results from the fundamental Faraday's law of induction, where ε is the electromotive force and B is the spatially uniform magnetic field. The variation of the magnetic flux, Φ, through an enclosed surface induces an electric vector field, which gives rise to an induced voltage defined as:

$$\varepsilon = -n\frac{d\Phi}{dt} = -n\,A\frac{dB}{dt} \qquad (2)$$

where A is the area of the coil and n is the number of turns. It is worth mentioning that inductive loops and loop antennas are both types of loop sensors that utilize loops of conductive material to generate or detect electromagnetic fields. However, they serve different purposes and have distinct characteristics. It is known that inductive loops are often used for near-field coupling in applications such as wireless power transfer and proximity sensing, while loop antennas

TABLE II. DIFFERENT INDUCTIVE LOOPS DIMENSIONS.

Loop	*D* (mm)	*d* (mm)	*n*	*w* (mm)	*s* (mm)
3	31.2	10.4	6	0.8	0.8
4	31.2	2.4	9	0.8	0.8
5	31.2	15.2	6	0.8	0.4
6	31.2	15.6	6	0.4	0.8

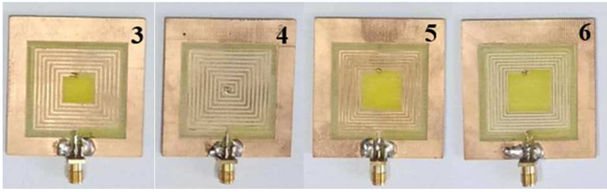

Fig. 3. Manufactured multi-turn inductive loops (from left to right loop-3, loop-4, loop-5, and loop-6).

are mainly used for radiating or receiving electromagnetic waves in far-field communication systems.

IV. PD SETUP AND DETECTION RESULTS

A defected MVAC single-core power cable with a conductor cross-section of 150 mm^2 and a length of 10 m was used as a PD source to assess the sensor's sensitivity to the presence of a discharge problem. To evaluate the performance of the designed PCB-based loop sensors, an experimental setup is elaborated to generate internal discharges, as reported in Fig. 4. It consists primarily of a 100 kV transformer, a capacitive voltage divider, and a faulty power cable. A voltage regulator, operating in the range of 0–400 V, was employed to determine the required AC–HV applied voltage. All the sensors were tied to the defected cable alternately, at the same distance of a few centimeters as shown in Fig. 4. The transformer's output voltage was increased using the DC regulator until PDs occurred, discernible by characteristic patterns appearing on the PC screen. Both ends of the defective cable were connected to the HVAC generator, with AC voltage applied to the core conductor while grounding the cable screen. The detected PD Inception Voltage (PDIV) result was 8.5 kV. All voltage outputs were recorded using a PicoScope 3000 Series (sampling frequency: 1 GS/s, 8-bit, and 100 MHz bandwidth) when using a 50 Ω coaxial cable. The PicoScope was connected to the computer using a USB cable to acquire and store the data from the PD measurement.

Fig. 5 illustrates the output voltage waveforms of the PD pulses and their frequency spectra detected by loop-1 and loop-5. Table III shows the peak-to-peak voltage values detected by each loop sensor and the frequency range of the main lobes present. As noted, the peak-to-peak voltage detected by loop-1 is 397.2 mV, while loop-2, which has the biggest diameter, exhibits an amplitude voltage of 34.6 mV. Furthermore, loop-1 and 2 show a large spectrum frequency starting from 10.2 to 152 MHz, while loop-3 to 6 have a unique fundamental frequency of about 40 MHz.

V. PARAMETERS EXTRACTION AND DISCUSSION

For single-turn loop antennas, Table III highlights that loop-1 is more sensitive to PD pulses than loop-2 despite its smaller circumference. However, in telecommunication, it is well known that the larger the circumference of the loop antenna compared to the intended operating wavelength (1 to100 MHz), the more effective it becomes. In fact, a larger

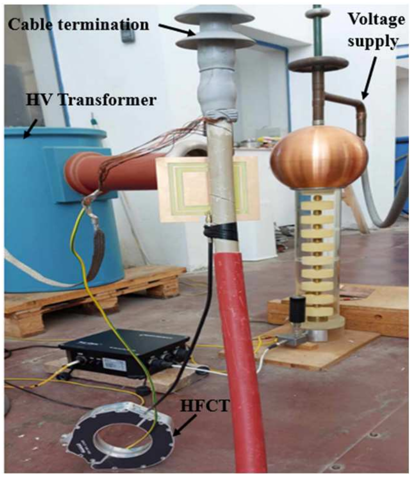

Fig. 4. Experimental setup for PD generation and detection.

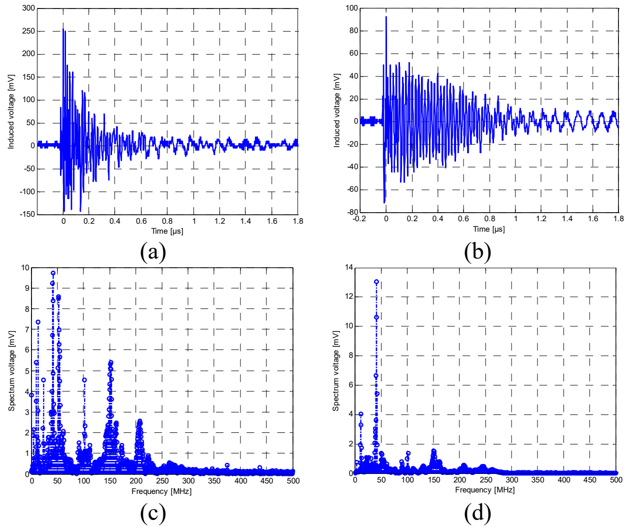

Fig. 5. (a)-(b) The time-domain waveforms due to PD detected by loop-1 and loop-5, and their (c)-(d) frequency spectrum.

TABLE III. PEAK-TO-PEAK VOLTAGE DETECTED BY DIFFERENT LOOPS.

Loop-	1	2	3	4	5	6
$V_{p\text{-}p}$ (mV)	397.2	34.6	179.6	174	164	136.4
Lobes frequency (MHz)	10.2–152	14.6–147.9	40.5–41.5	40.5–41	40–41	40.5–41.5

loop antenna typically exhibits higher radiation resistance, which is desirable for efficient power transfer. Recorded results contradict this theory, which leads us to conclude that the first two loops do not function as a loop antenna but rather as an inductive loop. To analyze and better understand the behavior of all sensors, Ansys HFSS software was used. A numerical extraction of the loops' lumped-element model was performed to compare the sensors' performances through their scattering parameters. These factors are useful for analyzing radio frequency sensors' performance and how to customize them for a particular use. Hence, inductance, *Q*-factor, and self-resonance frequency (SRF) are the three significant figures of merit that characterize spiral inductors. The *Q*-factor is the ratio of the energy stored in conservative (reactive) elements to the total dissipation (in non-conservative elements) per cycle for a sinusoidal excitation [11]. To confirm the simulation results, lumped-element parameters were also extracted from measurements using a

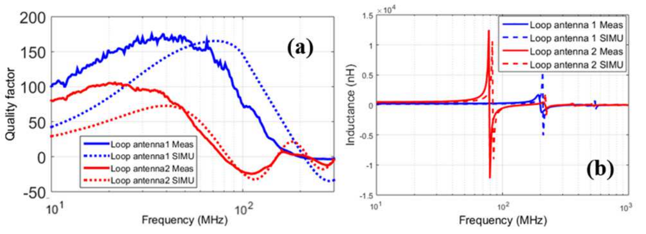

Fig. 6. Loop antennas (a) quality factors, and (b) self-inductance, extracted from HFSS simulation and measurements.

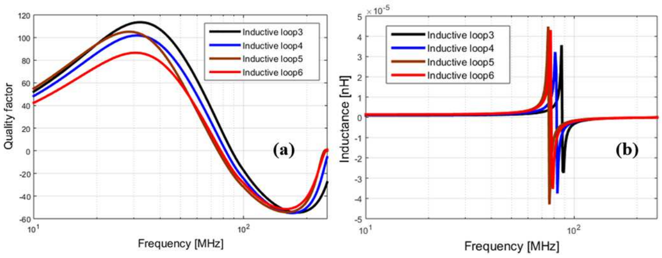

Fig. 7. Inductive Loops (a) quality factors, and (b) inductance, extracted from Ansys HFSS simulation.

TABLE IV. SIMULATED/MEASURED PARAMETER VALUES OF LOOP SENSORS.

Loop sensors		Parameters				
		SRF (MHz)	*L_s (µH) @ 10 MHz*	*R_s (Ω) @ 10 MHz*	*C_s (pF)*	Q_{max}
1	Meas	210	0.2	0.26	3	172
	Simu	200	0.19	0.2	3.02	169.2
2	Meas	79.4	0.49	0.8	6.9	100
	Simu	84	0.48	0.75	7.21	73
3	Meas	87	1.19	2.33	2.6	120
	Simu	87.5	1.176	2.37	2.8	113.5
4	Meas	82	1.3	2.16	2.9	115
	Simu	82	1.26	2.14	2.9	101.9
5	Meas	75	1.46	2.27	3	118
	Simu	75	1.44	2.26	3.1	105.12
6	Meas	77	1.5	2.5	2.7	90
	Simu	79	1.45	2.45	2.9	86.5

vector network analyzer (Keysight E5061B ENA, 100 kHz to 3 GHz). Fig. 6 illustrates the measured and simulated *Q*-factors and inductance of the two single-turn loop antennas 1 and 2. Although some differences appear due to the influence of the measurement environment and dimension variation, the SRF value is the same in both cases. The graphs illustrate that loop-1 exhibits the highest *Q*-factor, reaching 169.2@73 MHz, and the lowest inductance value (190 nH @10 MHz). Beyond 73 MHz, the *Q*-factor decreases, eventually dropping to zero at approximately 210 MHz, which corresponds to the loop's SRF. Loop-2 presents a simulated quality factor of around 73 @73 MHz and a SRF of around 79 MHz. Figs. 7a and 7b depict the simulated *Q*-factors and self-inductances of the four multi-turn inductive loops, respectively. For both curves, the results are relatively close to the simulation, and any difference is due to tiny differences in dimensions.

Table VI summarizes the simulated and measured parameter values of all the loop sensors. As we can see, all the results are fairly consistent. These results illustrate that loop-1 has the highest performance due to its highest *Q*-factor and SRF value, which extended the sensor bandwidth. Concerning the inductive loops, the detection capacity from the most sensitive to the least sensitive is as follows: loops-3, 5, 4, and 6. The highest *Q*-factor is observed for almost the same order. From these, an indication regarding the sensor's ability to detect PD signals can be assessed. Indeed, for these geometries, loop-3 has the better geometric dimensions since, in increasing the number of turns, as in the geometry of loop-4, we increase the electrical resistivity and then decrease the *Q*-factor. Besides, by decreasing the inter-spiral space, as in loop-5, the SFR will decrease since the stray capacitance will increase, which will reduce the sensor bandwidth. Finally, by decreasing the width of the track, as in loop-6, the resistivity of the sensor will increase significantly, and then the *Q*-factor will decrease. In conclusion, it could be recognized that the detection ability of all sensors is mainly related to their quality factor; the higher it is, the higher the peak voltage, thereby increasing the sensitivity of the loop sensor in the early detection of PD.

VI. CONCLUSION

In this paper, an investigation of six different PCB-based loop sensors, consisting of two single-turn loop antennas and four multi-turn inductive loops, to assess their sensitivity for PD detection is presented. Magnetic loop sensors provide an advantage over other antennas in terms of a smaller size, a higher quality factor, and a better signal-to-noise ratio. First, simulations with Ansys HFSS software and measurements are carried out to evaluate the equivalent lumped-element electrical model of all sensors and the figure or merit including the *Q*-factor. Then, the sensor ability of detecting PD on a defected MVAC single-core power cable was analyzed, leading to the conclusion that the single-turn loop antenna (loop-1) has the highest sensitivity. However, comparing the two loop antennas, it was found that although loop-1 had the smallest circumference, it provides the highest peak-to-peak induced voltage. This superiority is closely linked to the *Q*-factor improved by changes in sensor geometry.

REFERENCES

[1] F. Rozi and U. Khayam, "Development of Loop Antennas for Partial Discharge Detection," Int. J. Electr. Eng. Inform., vol. 7, no. 1, pp. 29–41, Mar. 2015.

[2] S. Kaziz, P. Romano, A. Imburgia, G. Ala, H. sghaier, D. Flandre, and F. Tounsi, "PCB-Based Planar Inductive Loops for Partial Discharges Detection in Power Cables," Sensors, vol. 23, no. 1, p. 290, Dec. 2022.

[3] T. Morozova, M. Demin, and A. Bondarchuk, "Concerning partial discharge detection in cable lines using high-frequency sensors," E3S Web Conf., vol. 390, p. 06030, 2023.

[4] L. Barbieri, A. Villa, R. Malgesini, D. Palladini, and C. Laurano, "An Innovative Sensor for Cable Joint Monitoring and Partial Discharge Localization," Energies, vol. 14, no. 14, p. 4095, Jul. 2021.

[5] S. Kaziz, A. Imburgia, D. Flandre, G. Rizzo, P. Romano, F. Viola, G. Ala, and F. Tounsi, "Performances of a PCB-based Loop Antenna Inductive Sensor for Partial Discharges Detection," IEEE International Conference on Dielectrics, Palermo, Italy, pp. 9–12, Jul. 2022.

[6] C. Suo, J. Zhao, X. Wu, Z. Xu, W. Zhang, and M. He, "Partial Discharge Detection Technology for Switchgear Based on Near-Field Detection," Electronics, vol. 12, no. 2, p. 336, Jan. 2023.

[7] A. Imburgia, S. Kaziz, P. Romano, D. Flandre, G. Artale, G. Rizzo, F. Viola, G. Ala, and F. Tounsi, , "Printed-Board Inductive Loop Topologies Performance for Partial Discharges Detection," IEEE Transactions on Industry Applications, pp. 1–8, 2024.

[8] N. Zeidi, S. Kaziz, M. H. Said, L. Rufer, A. Cavallini, and F. Tounsi, "Partial discharge detection with on-chip spiral inductor as a loop antenna," Rev. Sci. Instrum., vol. 92, no. 9, p. 094701, Sep. 2021.

[9] S. Kaziz, M. H. Said, A. Imburgia, B. Maamer, D. Flandre, P. Romano, and F. Tounsi, "Radiometric Partial Discharge Detection: A Review," Energies, vol. 16, no. 4, p. 1978, Feb. 2023.

[10] C. A. Balanis, "Antenna theory: analysis and design", 3rd ed. Hoboken, NJ: John Wiley, 2005.

[11] S. Kang, C.-K. Ding, C.-Y. Chen, and X.-Q. Wu, "High-Order Dispersion Coefficients for Alkali-metal Atoms," Commun. Theor. Phys., vol. 60, no. 1, pp. 73–79, Jul. 2013.